Heat, air and moisture transport modelling in ventilated cavity walls.

Marnix Van Belleghem, Marijke Steeman, Arnold Janssens and Michel De Paepe

In: Journal of Building Physics, Vol 38(4), pp. 317-349, 2015.

Van Belleghem M., Steeman M., Janssens A., De Paepe M. (2015) Heat, air and moisture transport modelling in ventilated cavity walls. Journal of Building Physics, Vol 38(4) 317-349.
doi: 10.1177/1744259114543984

Heat, air and moisture transport modelling in ventilated cavity walls

M. Van Belleghem[1], M. Steeman[2], A. Janssens[3] and M. De Paepe[1]

[1] Ghent University, Department of Flow, Heat and Combustion Mechanics, Sint-Pietersnieuwstraat 40, B-9000 Gent, Belgium
[2] Ghent University, Department of Industrial Technology and Construction, Valentin Vaerwijckweg 1, B-9000 Gent, Belgium
[3] Ghent University, Department of Architecture and Urban Planning, Jozef Plateaustraat 22, B-9000 Gent, Belgium

Corresponding author: Marijke Steeman
Department of Industrial Technology and Construction, Ghent University
Valentin Vaerwijckweg 1, 9000 Ghent, Belgium
Email: Marijke.Steeman@UGent.be

Keywords

Cavity wall, heat, air, moisture transfer, computational fluid dynamics, drying

Abstract

Cavity walls are a widely used external wall type in north-western Europe with a good moisture tolerance in cool humid climates. In this work, a cavity wall configuration with a brick veneer outside leaf and a wood fibre board inside leaf is analysed with a newly developed coupled computational fluid dynamics–heat, air and moisture model. Drying of the outside or inside cavity leaf, both for summer and winter conditions was analysed. The new model was compared with a widely used simulation tool for building envelope analysis (WUFI®) that uses a simplified modelling approach for the convection in the cavity. The study showed that the simplified model overestimated the drying and moistening rates of the cavity wall compared to the detailed model. For both models the drying of the outer leaf was mainly determined by the outside conditions, and the outside leaf dried out mainly to the outside and not to the cavity. For the inside leaf, however the cavity ventilation was of major importance in drying. The study revealed that the simplified model could not be used to evaluate the drying potential of a ventilated cavity because it overestimated the ventilation effect systematically. The simplified model would in such case indicate lower moisture contents than in reality and consequently lower risk for mould growth, wood rot or other structural damage. Only detailed modelling of the convection in the cavity, as in the new model, leads to a correct evaluation of ventilated cavity walls.

Introduction

The building envelope is constantly exposed to harsh environmental conditions. To prevent damage to the building and its envelope, a sophisticated design is often needed. A specific class of multilayer wall systems is the cavity wall. The main durability problems in cavity walls are frost damage, rain penetration and mould development. Their likeliness to occur is related to design flaws and workmanship imperfections. Hens et al. (2007) give a good overview of moisture-related problems in cavity walls. Cavity walls have a good moisture tolerance especially against the largest moisture source: wind-driven rain. The outside leaf acts as a weather barrier. Wind-driven rain hitting the wall is absorbed by the outside leaf if it is porous and capillary active (e.g. brick), the remainder runs off. Moisture that eventually reaches the cavity will runoff at the backside in the cavity. Drainage should be provided at the bottom of the wall to enable water evacuation from the cavity.
Besides acting as a capillary break and preventing moisture from outside to reach the inner wall, the ventilated cavity can also help to remove moisture from the inner cavity leaf. Salonvaara et al. (2007) conducted a literature review and found that not all authors agree on the effect of cavity ventilation. Hens et al. (2007) state that there is no real benefit of cavity ventilation. Without special measures, ventilation rates in the cavity will be low and drying of, for example, a brick veneer outside wall will mostly occur at the outside and less at the cavity side. Other studies indicate that cavity ventilation can increase drying (Straube, 1998), if ventilation rates are high enough. Some studies even report

negative effects of cavity ventilation. For instance, when the absolute humidity of the air flowing through the cavity is high, the moisture in the air results in a hygroscopic moisture loading.

This analysis clearly shows that the findings related to the benefits of cavity walls are contradictory. A wide range of building envelope types exist and an air cavity will not provide beneficial moisture and thermal performance for all. Furthermore, climate boundary conditions will determine to a great extent the performance of a cavity wall. A hygrothermal model could help researchers to gain a better understanding of the behaviour of cavity walls under different conditions and with varying configurations.

A cavity wall combines a lot of transport mechanisms and sources for heat and moisture, which explains the difficulty in modelling such a configuration. Figures 1 and 2 illustrate some of the main transport mechanisms for heat and moisture in ventilated cavity walls.

Figure 1 shows the heat fluxes, sources and sinks present in a cavity wall. For heat, three transport mechanisms can be identified: radiation, convection and conduction. At the outside, heat transport by radiation is very important. During sunny days, solar radiation accounts for a large part of the heat gains of the wall. Solar radiation is referred to as shortwave radiation. Next, heat exchange by longwave radiation is possible. This is radiation emitted by the wall or received from the surroundings. The wall will also exchange radiant heat with the sky. During clear winter nights, the temperature of the sky can be some 21°C lower than the environmental temperature (Hens, 2007). This can result in significant longwave radiant heat losses.

Heat transfer by longwave radiation occurs in the cavity when the cavity leafs have a different temperature. If convection in the cavity is low, the longwave radiation will be the most important heat transfer mechanism between the cavity leafs. Also at the indoor environment, longwave radiation from surrounding walls and objects can be of importance for the heat balance of the wall.

Air flow along the wall will result in convective heat transfer. Convection is transport by flow of a fluid, in this case air. Heat is transported from the wall surface to the air or from the air to the wall surface by the movement of air.

Transport through the (porous) solid cavity leafs is mainly by conduction. Conductive heat transport in the air is also present but will be small compared to convective transport.

Figure 2 illustrates the main moisture fluxes and sources in a cavity wall. Moisture sources depicted in Figure 2 are wind-driven rain, rising damp and outdoor and indoor vapour. This vapour is transported to the wall or in the cavity by convection and diffusion and can be absorbed in the porous wall. Moisture in the building envelope can result in mould growth, deterioration of building materials, wood rot and so on.

In literature, some simplified models for cavity ventilation can be found: for example, Karagiozis and Künzel (2009), Ge and Ye (2007) and Sanjuan et al. (2011). In this article, the impact of some of these simplifications on the heat, air and moisture (HAM) transport in a cavity wall is investigated. Therefore, a new coupled computational fluid dynamics–heat, air and moisture (CFD-HAM) model is developed and applied to a ventilated cavity wall. This model combines a detailed CFD model for the air transport in the cavity with an HAM model for the transport in porous materials. The new model is compared with a simplified commercially available model.

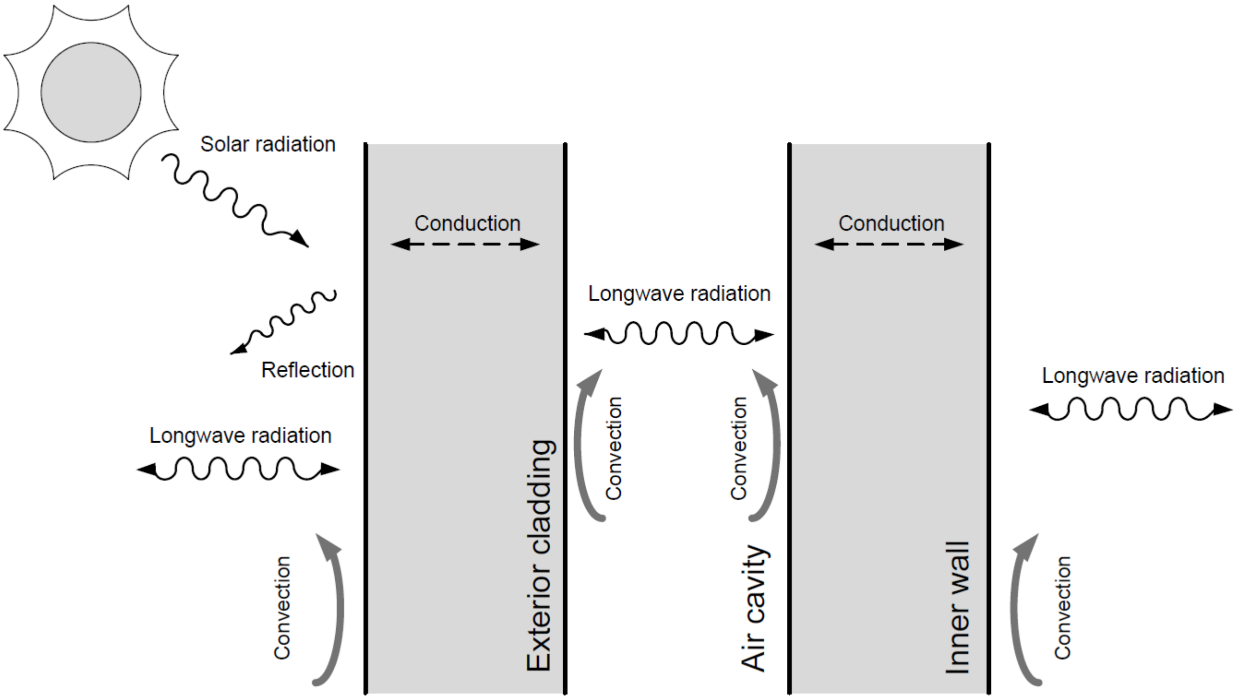

Figure 1. Illustration of heat fluxes occurring in and around a ventilated cavity wall

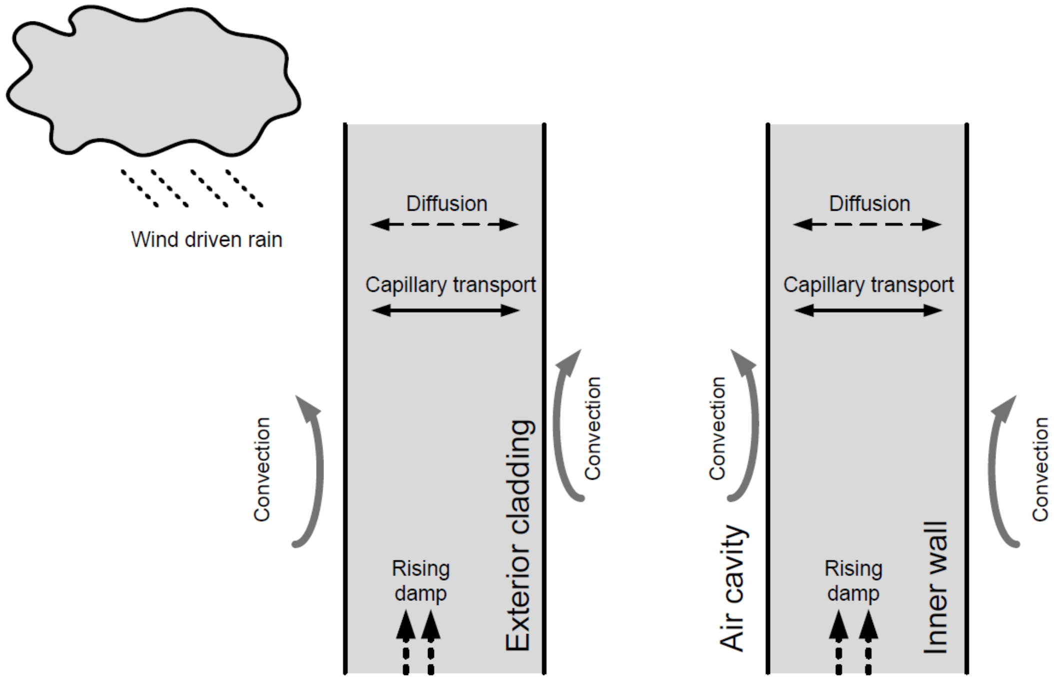

Figure 2. Illustration of possible moisture fluxes occurring in and round a ventilated cavity wall

Simplified ventilated cavity wall modelling

To model the impact of cavity ventilation on the building envelope performance, Straube and Finch (2009) and Finch and Straube (2007) listed some possible modelling techniques. They used a commercially available model (WUFI®; Zirkelbach et al., 2007) to calculate the HAM transport in a cavity wall. The simplest approach according to them is ignoring ventilation. The cavity is modelled as still air. The thermal conductivity of the air layer is adapted to incorporate radiation, conduction and natural convection effects in a non-ventilated cavity. This results in a thermal resistance of the cavity as function of the inclination and cavity width. The vapour resistance factor of the air layer was adapted to include the effect of vapour diffusion and convection. Straube and Finch, however, found that this approach yields inaccurate results and state that the ventilation effect should be included in the modelling.

A second approach reported by Straube and Finch (2009) and Finch and Straube (2007) is adjusting the vapour permeance of the exterior cladding. The user adapts the vapour permeance depending on the estimated ventilation rates.

In some cases, the external cladding can be removed from the model. This is valid if the conditions in the cavity are the same as those of the outside. However, the shielding effect of the external cladding for rain and solar radiation should still be included. Driving rain and solar radiation have a significant impact on the moisture transport in the cavity wall and these models tend to underestimate the moisture loading. This modelling approach can be improved by using measured cavity conditions as outside condition.

Nevertheless, the aforementioned modelling techniques tend to yield inaccurate results. Therefore, Karagiozis and Künzel (2009) developed a simplified model for cavity wall ventilation and implemented it in WUFI. The simplified model was able to capture the bulk performance of a cavity wall with reasonable accuracy and gave a rather good agreement with field data.

To account for ventilation, heat and moisture sources and sinks were added to the air layer. The moisture and heat added to or extracted from the cavity is modelled as a well-mixed process. The heat source/sink is determined as the amount of enthalpy entering the cavity minus the amount leaving the cavity due to ventilation. The mass source/sink is the mass entering minus the mass leaving the cavity. This can be expressed by the following equations

$$S_h = Q_{air}\rho\left(h_{ext} - h_{cavity}\right) \tag{1}$$

$$S_m = Q_{air}\left(\rho_{ext} - \rho_{cavity}\right) \tag{2}$$

where S_h and S_m are the heat and mass sources/sinks, respectively; Q_{air} is the volumetric air flow rate per volume of cavity (m^3/sm^3); h_{ext} and ρ_{ext} are the enthalpy and air density at the cavity entrance and h_{cavity} and ρ_{cavity} are the enthalpy and density at the cavity outlet, respectively.

The modelling techniques proposed by Karagiozis and Künzel (2009) strongly simplify the actual transport mechanisms in the cavity. In reality, air will enter the cavity through one of the cavity ventilation openings. The driving forces for the ventilation are the pressure difference due to wind pressure on the building façade and the pressure difference due to buoyancy. These pressure differences can fluctuate strongly in time. Also, changes in outside conditions over time such as outside temperature and radiation will affect the buoyancy forces in the cavity and thus alter the flow field in the cavity.

At the same time, heat and mass transfer from the cavity leafs to the cavity is determined by the flow field in the cavity. There is thus a strong coupling between the external conditions and the flow field in the cavity on the one side and between the flow field and the heat and mass transfer to the cavity on the other side. Karagiozis et al. neglect this coupling and state that assuming an averaged ventilation rate in the cavity often suffices.

Even if the ventilation rate is assumed to be constant, the flow field in the cavity would still change due to varying boundary conditions. In the simplified model implemented in WUFI, the impact of convection as transport mechanism in the cavity is included in the adjusted thermal conductivity and vapour diffusivity. These values are, however, constant and their determination is based on natural convection in a closed cavity. It is clear that these parameters do not include the impact of varying boundary conditions since they do not change in time and/or space.

The assumption of constant flow conditions in the cavity is to some extent justifiable. Air velocity in the cavity is low and heat transport is mostly determined by radiation. If there is an initial difference in temperature between the cavity walls, this difference will disappear due to the radiant heat exchange

between both surfaces. Since temperature differences are equalized in the cavity, the impact of buoyancy on the flow field will be less.
Simultaneously, the diffusion of water vapour from and to the cavity leafs is determined by the vapour diffusion resistance of the porous materials which is often larger than that of air. This again reduces the impact of the flow conditions in the cavity on the convective transport from cavity walls to cavity and explains why the simplifications introduced by Karagiozis and Künzel (2009) still result in reasonable agreement with measurements.
However, there are some cases where the previously listed assumptions no longer apply, for example, if a cavity wall is saturated with water and dried by convection. During the first drying stage, when the drying rate is constant, the moisture transport is determined by the convective boundary conditions. In order to accurately predict the drying of a wet cavity, it is thus important to capture the convective boundary conditions in the cavity with a reasonable accuracy. Furthermore, simplified models such as WUFI neglect the development of boundary layers in the cavity and the resulting distribution of convection coefficients. For example, if air enters a cavity wall at the bottom, boundary layers will be thin at that point and fluxes from porous material to cavity will be higher. For a wet wall, this means that the wall will dry out faster at the bottom than at the top if air enters at the bottom.
It is not clear to what extend the simplifications proposed by Karagiozis and Künzel (2009) hold. It is thus interesting to develop a model for heat and mass transport in a cavity, with a more detailed modelling of convection in the cavity. In the next section, this model will be discussed before studying in more detail the impact of some of the simplifications used in WUFI.

Coupled heat, air and mass transfer model

In this article, a conjugate modelling approach of the heat and moisture transport in the air and porous material is developed and discussed. Heat and moisture transport in the air is solved together with the transport in the porous material. A special coupling procedure is used to assure heat and mass flux continuity and temperature and mass fraction continuity at the air–porous material interface. The newly developed model can be applied to study a ventilated cavity wall in a detailed way.

Heat and moisture transport in the air

The transport equation for heat and moisture transport in the air was already developed by Steeman et al. (2009) and discussed in Van Belleghem et al. (2010, 2011). In this article, only a short overview of the governing equations is given. First, moisture transport in the air is discussed, next the heat transport will be elaborated. Moisture is transported in air as water vapour. This water vapour can be transported through air by convection and diffusion. Water vapour diffusion in air can be described by Fick's law of diffusion (Welty et al., 2001). Fick stated that the diffusion mass flux of component A (in this case water vapour) into component B (air) is proportional to the gradient of the mass fraction of component A

$$\vec{g}_v = -\rho D_{va} \nabla Y \tag{3}$$

Y is the mass fraction of water vapour in air (kg/kg), D_{va} is the diffusion coefficient of water vapour in air (m^2/s), ρ is the density of the air–vapour mixture (kg/m^3) and g_v is the water vapour diffusion flux (kg/m^2 s). The molecular diffusion of water vapour in air D_{va} is given by equation (4) (Schirmer, 1938)

$$D_{va} = 2.31 \times 10^{-5} \frac{101325}{P_{op}} \left(\frac{T}{273.16}\right)^{1.81} \tag{4}$$

The effect of turbulence on the diffusion can be incorporated by introducing a turbulent diffusion coefficient D_t. The ratio between the turbulent viscosity and the turbulent diffusivity is given by the turbulent Schmidt number. A number of experiments showed that this Schmidt number can often be assumed constant (Versteeg and Malalasekara, 2007). For this work, a value of Sc_t=0.7 is assumed

$$Sc_t = 0.7 = \frac{\nu_t}{D_t} \tag{5}$$

Combining the turbulent diffusion coefficient and the molecular diffusion results in an effective diffusion coefficient D_{eff}. The differential form of the moisture transport equation in air is then given by

$$\frac{\partial}{\partial t}(\rho Y) + \nabla \cdot (\rho \vec{v} Y) = -\nabla \cdot \vec{g} = \nabla \cdot \left(\rho D_{eff} \nabla Y\right) \tag{6}$$

To model the transport of heat in air, an energy transport equation is needed. This energy equation is found by writing down the energy balance for a control volume. This energy balance states that the change in total internal energy in time is due to heat transported through the boundaries of the control volume along with the flow and due to heat transported through the boundaries by diffusion. This diffusion incorporates the conduction of heat and the transport of sensible and latent heat due to water vapour diffusion. This implies that there is a coupling of the heat transport equations and the water vapour transport. In the development of the heat transport equations, some assumptions and simplifications were made as follows:

- The air is assumed incompressible;
- Pressure variations are small so they do not affect thermodynamic properties;
- Potential energy changes are assumed negligible;
- Kinetic energy changes are neglected;
- Viscous heating is neglected;
- No volumetric source terms are present (e.g. chemical reactions, droplet evaporation, condensation).

This results in the following equation for the conservation of heat

$$\frac{\partial}{\partial t}[\rho_a h_a + \rho_v h_v] + \nabla \cdot [(\rho_a h_a + \rho_v h_v)\vec{v}] = -\nabla \cdot [\vec{q} + h_a \vec{g}_a + h_v \vec{g}_v] \tag{7}$$

Here, h_a and h_v are the specific enthalpy of dry air and water vapour, respectively (J/kg). g_a and g_v are the diffusion fluxes of air and water vapour (kg/m^2 s) and q is the conductive heat flux (W/m^2). It is, however, more convenient to transform this equation so that the transported variable becomes the temperature T. This is possible by assuming the fluid incompressible

$$\begin{aligned}&\frac{\partial}{\partial t}[\rho(1-Y)C_a T + \rho Y(C_v T + L)] + \nabla \cdot \left[\vec{v}\left(\rho(1-Y)C_a T + \rho Y(C_v T + L)\right)\right]\\ &= \nabla \cdot \left[\lambda \nabla T - \left(-C_a T + (C_v T + L)\right)\vec{g}\right]\end{aligned} \tag{8}$$

The following assumptions are made to transform equation (7) into equation (8):

- The air is assumed incompressible;
- The internal energy of an incompressible fluid is only function of the temperature;
- For incompressible fluids, the heat capacity at constant volume c_v and constant pressure c_p (J/kg K) is assumed equal;
- Since temperature changes are small, the specific heat can be assumed constant;
- The conductive heat flux is determined by Fourier's law of conduction

$$\vec{q} = -\lambda \nabla T \tag{9}$$

- The diffusion of species A into species B is always accompanied by diffusion of B in the opposite direction. The net total amount of molar fluxes due to diffusion is zero. For a dilute gas mixture, it is a good approximation to assume that also the net total amount of mass fluxes is zero

$$\vec{g_v} = -\vec{g_a} \tag{10}$$

Similar to the turbulent vapour transport equation (equation (6)) where a turbulent diffusion coefficient was defined to account for the effect of turbulence on the diffusion transport, a turbulent conductivity λ_t can be defined. This turbulent conductivity is given by equation (11)

$$\mathrm{Pr_t} = \rho C \frac{\nu_t}{\lambda_t} \tag{11}$$

$$\lambda_{eff} = \lambda + \lambda_t$$

$\mathrm{Pr_t}$ is the turbulent Prandtl number which can be assumed constant and equal to 0.85.

L represents the latent heat of water evaporation at a reference temperature of 0°C. This allows bringing L outside the derivative operators in equation (8). When applying equation (6) to equation (8), the latent heat cancels out of the equation. This is as expected since no phase change (condensation/evaporation) is present in the air flow. The heat transport equation can thus be rewritten as

$$\frac{\partial}{\partial t}[\rho C T] + \nabla \cdot [\vec{v}(\rho C T)] = \nabla \cdot \left[\lambda_{eff} \nabla T - (C_v - C_a)\vec{g} T\right] \tag{12}$$

with the mass-weighted heat capacity given by

$$C = Y C_v + (1 - Y) C_a \tag{13}$$

Heat and moisture transport in porous materials

Moisture in a building context can exist in three phases: vapour, liquid and solid (ice). In the present model, ice and ice formation are neglected. The two remaining phases can both be stored and transported in a porous material. The moisture content in the porous material w (kg/m^3) is the sum of the vapour content w_v and the liquid content $_{wl}$. The vapour content is much smaller than the liquid content and is often neglected. The moisture flux in the material g (kg/m^2 s) is the result of a vapour flux g_v and liquid flux g_l. This is of course only an approximation since both transport mechanisms can strictly speaking not be divided. Convection of air in the porous material is neglected. The vapour diffusion flux in a porous material can be described by an adjusted Fick's diffusion law

$$\vec{g_v} = -\frac{D_{va}}{\mu R_v T} \nabla p_v \tag{14}$$

In equation (14), the total pressure is assumed constant, allowing the use of vapour pressure instead of mass fraction as driving force. m is the ratio of the vapour diffusion of water vapour in the porous material to the vapour diffusion of water vapour in air. This ratio is also referred to as the water vapour diffusion resistance factor. In these equations, for diffusion the thermal diffusion or Soret effect is neglected. It was stated in Waananen et al. (1993) and shown by Whitaker (1988) and Janssen (2011) that this effect is small compared to the concentration diffusion.
The liquid flux is described by Darcy's law

$$\vec{g_l} = -K_l \nabla p_c \tag{15}$$

The driving force for the liquid transport is the gradient in capillary pressure p_c (Pa). K_l is the liquid permeability (s). The moisture transport equation then results in

$$\frac{\partial w}{\partial t} = \nabla \cdot (\vec{g}_v + \vec{g}_l) = \nabla \cdot \left(\frac{D_{va}}{\mu R_v T}\nabla p_v + K_l \nabla p_c\right) \tag{16}$$
$$\Leftrightarrow \frac{\partial w}{\partial p_c}\frac{\partial p_c}{\partial t} = \nabla \cdot (\mathrm{K}_l \nabla \mathrm{p}_c) + \nabla \cdot \frac{D_{va}}{\mu R_v T}\left(\frac{\rho_v}{\rho_l}\nabla \mathrm{p}_c + RH\frac{\partial p_{sat}}{\partial T}\nabla \mathrm{T} - \frac{p_v \ln RH}{T}\nabla T\right)$$

The vapour pressure is transformed to the capillary pressure using Kelvin's law

$$p_v = \rho_l R_v T \ln RH \tag{17}$$

To solve equation (16), three material properties are needed: the vapour diffusion resistance factor μ, the liquid permeability K_l and the moisture capacity $\partial w/\partial pc$. For the materials used in the case study in section 'Drying of the ventilated cavity wall under summer and winter conditions', these properties are listed in Appendix 1.
Only transport by diffusion is assumed in the here studied porous materials. Heat is thus only transported in the porous materials due to conduction on the one hand and diffusion of water on the other hand. Water vapour diffusing through the porous materials transports sensible as well as latent heat.
Heat transport in a (porous) material due to diffusion can be described by Fourier's law of heat conduction

$$\vec{q} = -\lambda_{mat}\nabla T \tag{18}$$

λ_{mat} is the conductivity of the porous material (W/m K). This conductivity is strongly dependent on the moisture content of the material since the conductivity of water differs from that of the material matrix.
Water is transported through a porous material as liquid and vapour resulting in a liquid and vapour flux. Along with the liquid water, sensible heat is transported while sensible and latent heat are transported along with the vapour diffusion.
The potential energy and kinetic energy changes in the porous material can be neglected and no chemical reactions occur in the material. The total energy of the porous material E (J/m^3) is thus the sum of the energy stored in the material matrix and the energy stored in the liquid water and water vapour present in the material. The energy balance equation which states that a change in stored energy is only due to heat diffusion then becomes

$$\begin{aligned}\frac{\partial E}{\partial t} &= \frac{\partial}{\partial t}(\rho_{mat}h_{mat} + w_l h_l + w_v h_v) = \\ &(\rho_{mat}C_{mat} + w_l C_l + w_v C_v)\frac{\partial T}{\partial t} + C_l T\frac{\partial w_l}{\partial t} + (C_v T + L)\frac{\partial w_v}{\partial t} \\ &= \nabla \cdot (\lambda_{mat}\nabla T - C_l T g_l - (C_v T + L)\vec{g}_v)\end{aligned} \tag{19}$$

where w_v is the vapour moisture content and w_l is the liquid moisture content. ρ_{mat} is the dry porous material density (kg/m^3) and C_{mat} the heat capacity of the dry material (J/kg K).
The liquid moisture content and vapour moisture content can be linked to the total moisture by the open porosity ψ_0, taking into account that $w=w_l + w_v$ and $\psi_0=w_l\backslash\rho_l + w_v\backslash\rho_v$.

Numerical implementation
Generally, a calculation domain is divided into two zones: a porous material zone and an air zone. Since a different transported variable is used for the moisture transport in air and porous material, a coupling procedure for the boundary conditions is needed between the air and the material zone.
Four continuity conditions have to be fulfilled when the air and material zone are coupled:

- Continuity of temperature at the boundary: the temperature at the air side boundary T_{sa} should equal the temperature at the material side boundary T_{sm}. Thus, $T_{sm}=T_{sa}=T_s$;
- Continuity of the heat flux at the boundary: heat conduction in the porous material to the surface equals the convective heat leaving the surface;
- Continuity of mass fraction at the boundary: the mass fraction at the material side of the air–material interface Y_{sm} equals the mass fraction at the air side Y_{sa}. This means that $Y_{sa}=Y_{sm}=Y_s$;
- Continuity of moisture flux at the boundary.

Figure 3 illustrates the general coupling procedure applied in this work which fulfils the four continuity conditions for the boundary values and fluxes. First, the air side is calculated based on the material boundary conditions which are the mass fraction at the boundary Y_s and the temperature at the boundary T_s. When the temperature and mass fraction distribution in the air are known, the heat and mass flux from porous material to air can be determined using equations (20) and (21)

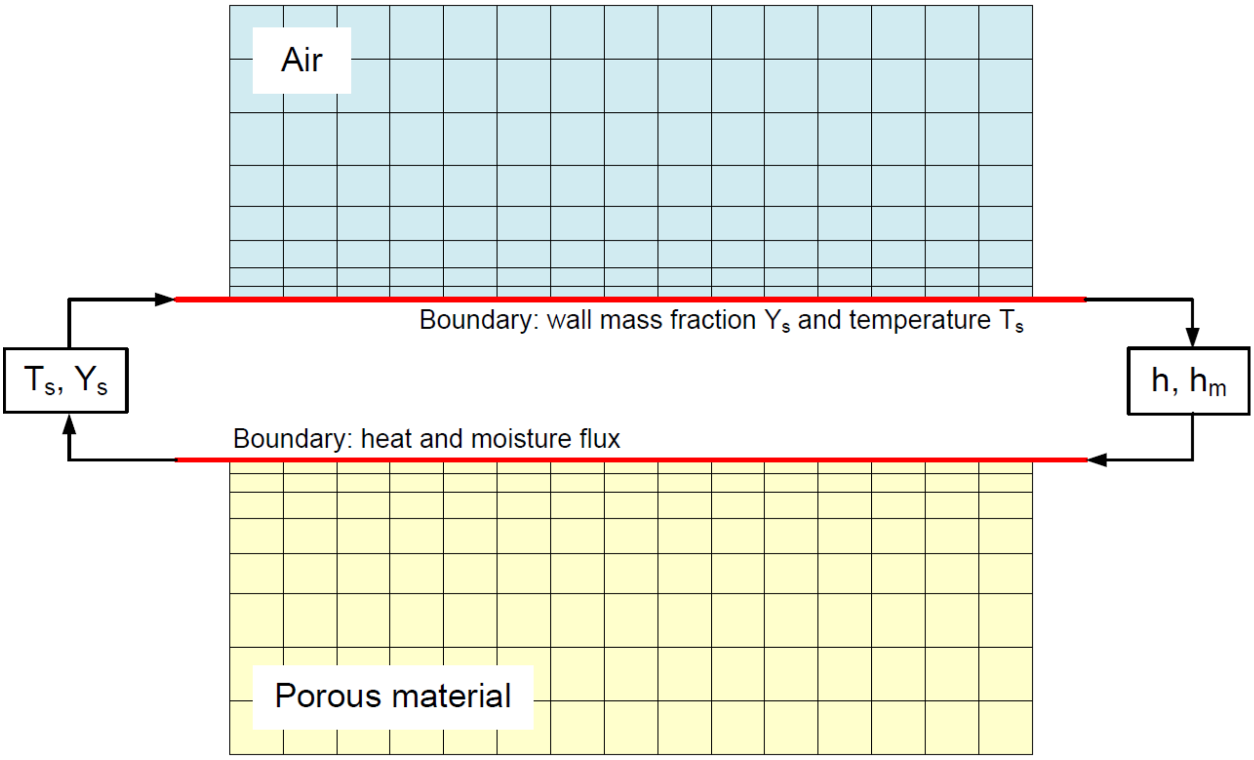

Figure 3. Schematic representation of the boundary conditions in the coupled CFD-HAM model. CFD-HAM: computational fluid dynamics – heat, air and moisture.

$$g_v = \rho D_{va} \frac{Y_{C0_a} - Y_s}{dr_a} \quad (20)$$

$$q = \lambda \frac{T_{C0_a} - T_s}{dr_a} \quad (21)$$

These equations are the discretized form of Fick's law (equation (3)) and Fourier's law (equation (9)). In these equations, Y_{C0a} and T_{C0a} are the mass fraction and temperature in the first cell next to a material cell, and Y_s and T_s are the mass fraction and temperature at the air–material interface. dr_a is the distance between the air–material interface and the cell centre of the first air cell adjacent to the interface.

The calculated heat and mass fluxes are used as boundary conditions for the porous material. Such a coupling procedure was also used by Defraeye et al. (2012). Defraeye, however, used two separate solvers, one for the transport in the air (Fluent 6.3; Fluent Inc., 2006; a commercial finite volume based program) and one for the transport in the porous material (heat, air and moisture finite element model (HAMFEM); Janssen et al., 2007; an in-house finite element–based program). The model discussed in this article uses only one solver (Fluent). The transport in the porous material is implemented into the CFD solver as additional equations.

Defraeye et al. (2012) used an explicit coupling procedure. First, the transport in the air was calculated for one time step, and from this calculation, the fluxes from material to air were determined. These fluxes were then passed to the porous material model where the same time step was calculated with fixed fluxes at the boundary during that time step. This iteration procedure is only possible if the time steps are sufficiently small and if the fluxes do not change significantly during a time step. This results in a computationally expensive procedure due to the small time steps that are needed.

An implicit solver method could overcome some of these issues. Therefore, an adopted coupling method is proposed in this work. Instead of using the calculated fluxes directly, transfer coefficients are determined with these fluxes, and these transfer coefficients are passed to the material side. A similar method was also proposed by Saneinejad et al. (2012). The transfer coefficients can be calculated using equations (22) and (23)

$$q = \alpha\left(T_{ref} - T_s\right) \tag{22}$$

$$g = \beta\left(Y_{ref} - Y_s\right) \tag{23}$$

In these equations, reference values for temperature (T_{ref}) and mass fraction (Y_{ref}) have to be determined. α is the heat transfer coefficient (W/m^2 K) and β is the mass transfer coefficient (s/m). The definition of these reference values can differ from case to case. For flow over a flat plate, the bulk temperature and mass fraction are often used as reference. Saneinejad et al. (2012) used the average values of temperature and concentration.

For more details about the numerical coupling between the HAM model and the CFD model, the reader is referred to Van Belleghem et al. (2014).

Ventilated cavity wall model

In this article, the coupled CFD-HAM model that is discussed in the previous section is applied to a ventilated cavity wall. Figure 4 shows an example of a cavity wall configuration. This configuration will be used for a more detailed study on heat and moisture transport. The cavity wall has an outside leaf of ceramic brick, an air cavity of 5 cm and an inside leaf of wood fibre board (Celit®, ISOPROC), mineral wool insulation and gypsum board as inside finishing. Some material properties of these materials are listed in Table 1. The moisture transport properties such as vapour diffusion coefficient and moisture retention curve are listed in Appendix 1 of this article.

The cavity wall is modelled as two parallel plates. For two parallel plates, there is no longer a clear definition of bulk flow since the boundary layers from both surfaces interfere. Therefore, as reference in equations (22) and (23), the temperature and mass fraction at a specified distance from the wall are used. This is indicated by the dashed line in Figure 4. So for each wall face, there is a different reference, the cell value being at a fixed normal distance from the face.

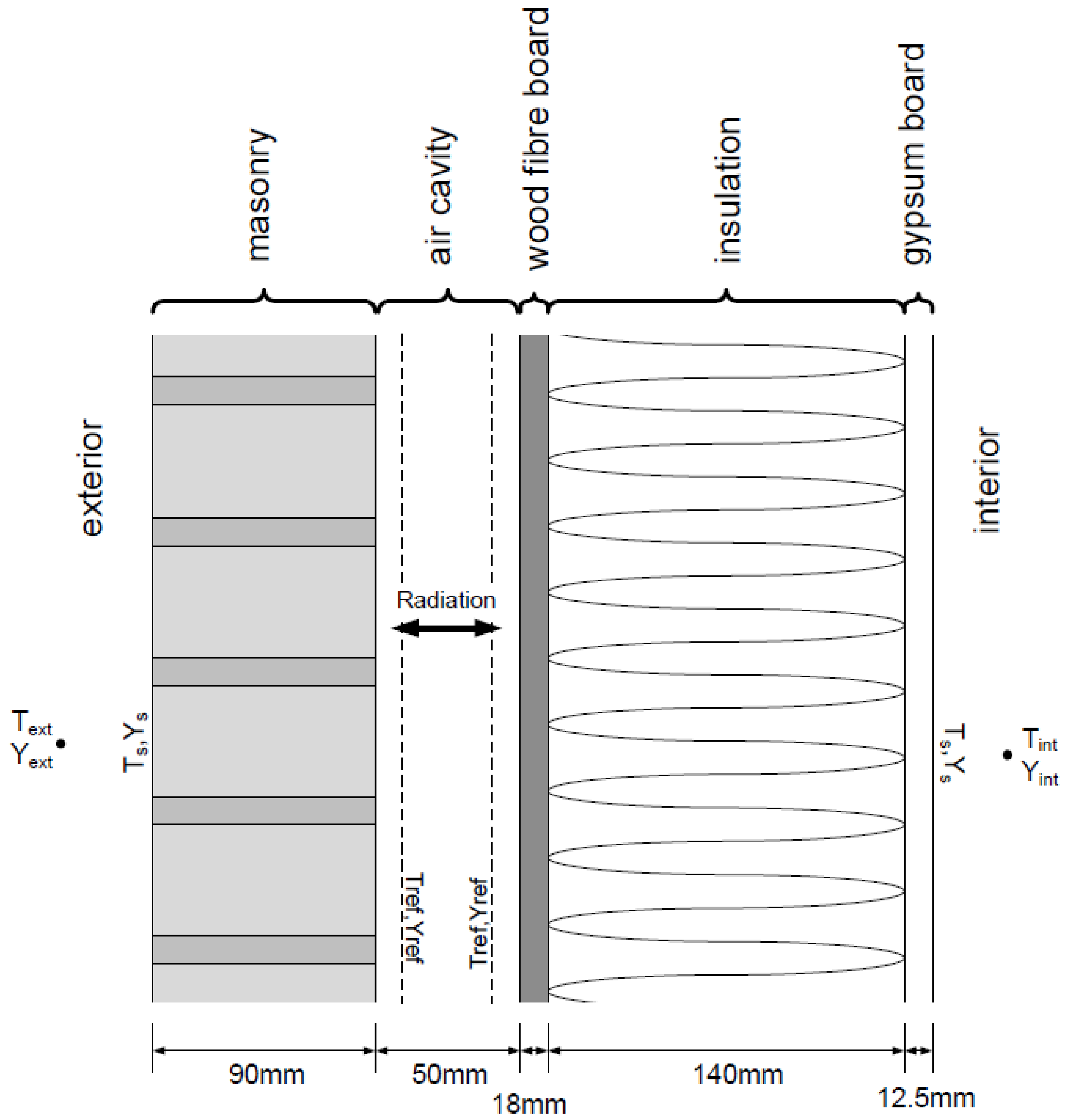

Figure 4. Cavity wall configuration

A velocity inlet at the bottom of the cavity is used, and at the top, a pressure outlet is assumed. Inlet temperature and mass fraction are based on the exterior weather conditions. As outside conditions, the climate in Brussels is used, based on data from Meteotest (2012). Two cases will be studied here, a warm summer day in June and a colder day in December. Temperature and relative humidity (RH) on the 20 June in Brussels are used as summer condition, and on the 17 December for winter conditions (Figures 5 and 6). The solar radiation is taken from Hens (1997) and is the maximum solar radiation for a clear sky on a vertical west facade during June and December, respectively. Figure 7 shows the daily variation in the solar radiation for the 20 June and the 17 December.

Table 1. Hygrothermal material properties, based on Derluyn et al. (2008), Desta et al. (2011) and Roels (2008). The properties of mineral wool were provided by the manufacturer.

Property	**Ceramic brick**	**Wood fibre board**	**Mineral wool**	**Gypsum board**
ρ [kg/m³]	2087	270	60	690
C_{mat} [J/kgK]	840	1550	1470	840
λ [W/mK]	1+0.0047w	0.048	0.023	0.198
μ_{dry} [-]	24.79	6	-	10.68
w_{cap} [kg/m³]	130	162	-	295
ψ_0 [-]	0.13	0.83	-	0.419

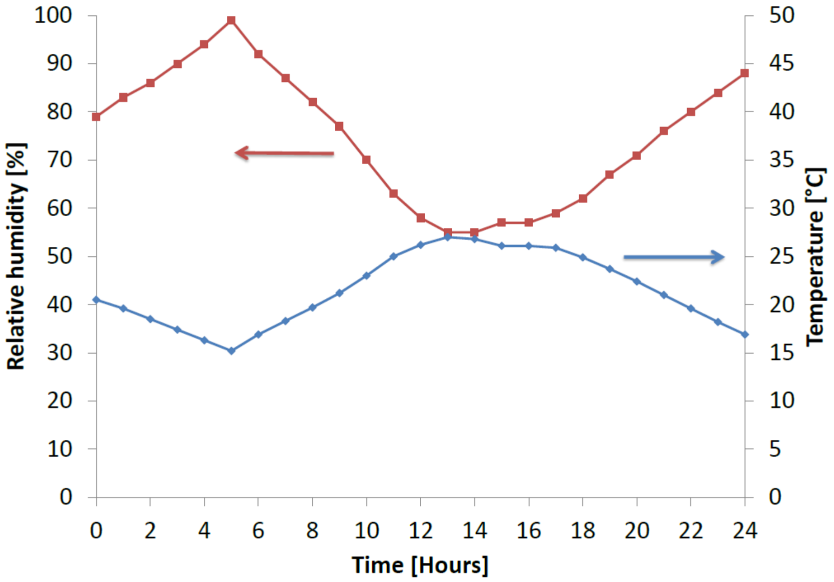

Figure 5. Temperature and RH for a summer day
RH: relative humidity.

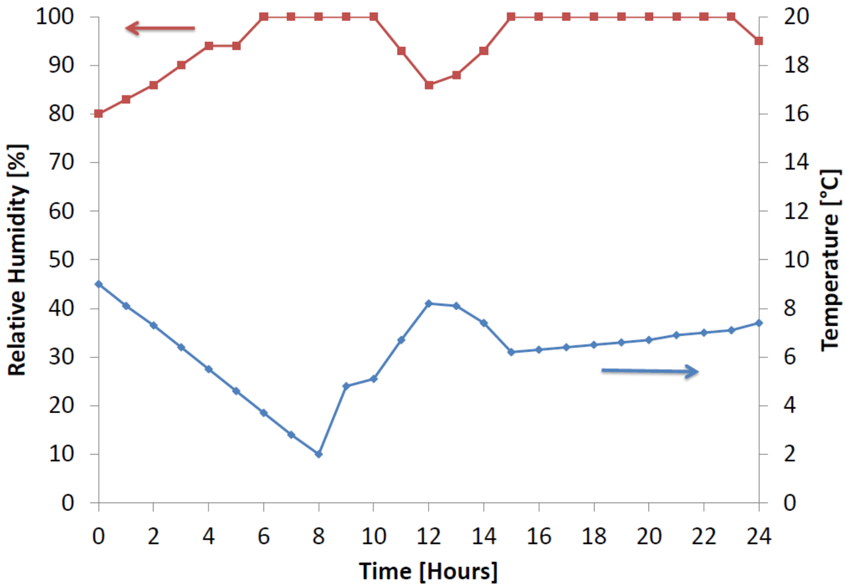

Figure 6. Temperature and RH for a winter day
RH: relative humidity

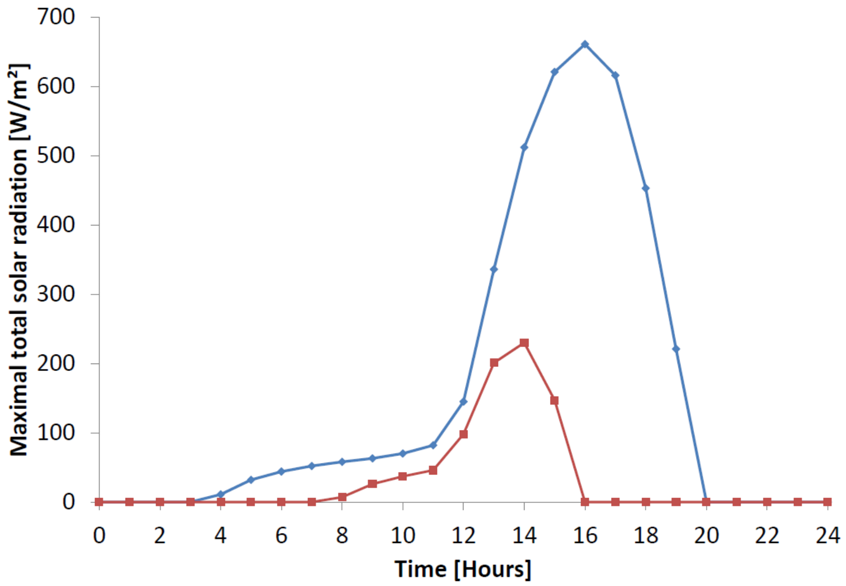

Figure 7. Total solar radiation

These conditions are used as exterior conditions for the ceramic brick outside leaf and as inlet conditions for the air cavity. The convective heat and mass transfer coefficients at the exterior wall surface were taken to be constant. The exterior heat transfer coefficient is 19W/m^2 K, and the mass transfer coefficient is 0.0217 s/m (which is within the range suggested by the American Society of Heating, Refrigerating and Air Conditioning Engineers (ASHRAE); Künzel et al., 2009). As interior conditions for the cavity wall, 21°C is used as constant room temperature and 50% RH as constant room RH. The convective heat and mass transfer coefficients at the interior wall are 8W/m^2 K and 0.00915 s/m, respectively.

Different time scales are present when HAM transport in porous materials is modelled. Transport phenomena in the air have a much smaller time constant than phenomena in porous materials. It is thus not necessary to model all time variations in the air, since fluctuations in the air with high frequency will have no impact on the heat and moisture transport in the material. Therefore, the air can be modelled as quasi-steady state. This implies that flow unsteadiness is neglected. The flow field can

be assumed constant during the time step if this time step is not too large. Changes in the flow field by changing boundary conditions are, however, still included.
The time step size used for the simulations with the coupled CFD-HAM model was 60 s. This value is based on earlier simulations with the coupled CFD-HAM model in Van Belleghem et al. (2010) and Van Belleghem et al. (2011) and gave good results.

With the coupled CFD-HAM model, it is possible to include convective transport in the cavity more accurately. However, convective transport is not the only transport mechanism in a cavity. Figure 1 shows the different heat transport mechanisms present in a cavity wall. Air velocity in a ventilated cavity wall is generally low. As a result, the convective heat transport is low and heat transfer due to longwave radiation will start to play a major role at these low velocities. Therefore, a surface-to-surface radiation model (view factor model) is added to the coupled CFD-HAM model to take into account longwave radiation in the cavity.
Since the cavity leafs are parallel and the cavity leaf dimensions are large compared to the cavity width, the radiation surfaces can be modelled as two infinite parallel plates. In this case, the view factors become 1. The net radiation from a cavity leaf reduces to

$$q_{rad} = \frac{1}{\frac{1}{\varepsilon_1}+\frac{1}{\varepsilon_2}-1}\left(T^4_{rad,avg,1} - T^4_{rad,avg,2}\right) \tag{24}$$

where ε_1 is the emissivity of the first cavity leaf and ε_2 is the emissivity of the second cavity leaf. $T_{rad,avg}$ is the surface-averaged radiation temperature of the cavity leaf. Here, the assumption is made that the surface temperature used for the radiation calculation is uniform. In reality, a distribution of the surface temperature will be present due to a combination of convection, conduction and radiation effects.

Drying of the ventilated cavity wall under summer and winter conditions

To evaluate the performance of a simplified cavity model, a cavity wall configuration under specific boundary conditions was simulated for a period of 1 day with WUFI-2D (Zirkelbach et al., 2007) and compared with simulations performed with the coupled CFD-HAM model. Figure 4 shows the cavity wall configuration that is used. The simulations were performed under summer and winter boundary conditions.
In total, five simulation cases are studied. Table 2 summarizes the initial conditions used for both the simplified (WUFI) and detailed (coupled CFD-HAM) simulation model:

- Case 1. Summer conditions are used. The outside cladding, composed out of a brick veneer wall, is assumed initially saturated with water. This mimics the situation after an intensive rain shower.
- Case 2. Winter conditions are used. The outside cladding is assumed initially saturated with water. Sky radiation during the night is neglected.
- Case 3. Summer conditions are used. This case is similar to case 1, only the moisture content of the wood fibre board differs. The wood fibre board is, similar to the brick, initially assumed saturated with water. This situation mimics, for example, rain penetration to the inside leaf or water leakage resulting in a wet inside leaf.
- Case 4. This case resembles case 3; only here, winter conditions are used as boundary conditions. The same initial conditions are used as in case 2.
- Case 5. A constant pressure inlet at the bottom of the cavity is assumed instead of a constant inlet velocity. The other boundary conditions are similar as those in case 3.

Case 1: summer conditions – non-saturated wood fibre board

In the first case, three inlet air velocities were evaluated: 0.1, 0.2 and 0.3 m/s. These velocities correspond to ventilation rates of, respectively, 144, 288 and 432 ACH (air changes per hour). These air change rates were used as input for the simplified WUFI model.

The estimation of the inlet velocity is based on a study by Jung (1985) reported in Straube (1998). In this study, a ventilation velocity of about 0.1 m/s was found for an average wind speed of 2.6 m/s. Therefore, in this study, ventilation velocities of similar magnitude are used.

It should, however, be noted that ventilation velocities of 0.1 m/s or higher, although common for large ventilation vents, are rare in brick veneer cavity walls with only a few open head joints. The hereinafter reported research results are thus only valid for well-ventilated cavity walls.

Constant velocities at the inlet were assumed so the air change rate in the cavity is also constant over time. Temperature and moisture gradients in the cavity, however, result in a redistribution of the velocity profile in the cavity due to buoyancy. This distribution changes in time since the temperature and moisture distribution in the cavity change. This results in transfer coefficients that strongly vary in time and space. The simplified model does not take these variations into account as mentioned in section 'Simplified ventilated cavity wall modelling'.

Figure 8 compares the results of the coupled CFD-HAM model with the results of the simplified model (WUFI) for case 1. In Figure 8(a), the moisture content in the brick veneer is depicted. Both models clearly show the same trends. Drying starts slow as the temperature of the surroundings and cavity is low and the RH in the air is still high. At sunrise, the temperatures gradually rise and solar radiation further heats up the cavity, which increases the drying rate. This can be seen in the larger slope of the moisture content graph after 10 a.m.

However, an overestimation of the drying rate by the simplified model compared to the coupled CFD-HAM model can be noticed. Table 3 compares the maximum relative difference of the moisture content simulated with the simplified model and with the coupled CFD-HAM model for each case. The relative difference is determined by dividing the absolute difference by the moisture content predicted by the CFD-HAM model. At an inlet velocity of 0.2 m/s, a maximum difference of 9.4% is found.

Table 2. Overview of boundary conditions and initial conditions used in the studied cases

		Case 1	**Case 2**	**Case 3**	**Case 4**	**Case 5**
		Summer	*Winter*	*Summer*	*Winter*	*Summer*
Brick		*Saturated*	*Saturated*	*Saturated*	*Saturated*	*Saturated*
	$T_{initial}$	18°C	9°C	18°C	9°C	18°C
	$RH_{initial}$	99.99%	99.99%	99.99%	99.99%	99.99%
	$w_{initial}$	129.7 kg/m³	129.7 kg/m³	129.7 kg/m³	129.7 kg/m³	129.7 kg/m³
Air cavity		*Constant inlet velocity*	*Constant inlet velocity*	*Constant inlet velocity*	*Constant inlet velocity*	*Constant inlet pressure*
	$T_{initial}$	25°C	9°C	25°C	9°C	25°C
	$RH_{initial}$	50%	80%	50%	80%	50%
Wood fibre board		*Not saturated*	*Not saturated*	*Saturated*	*Saturated*	*Saturated*
	$T_{initial}$	25°C	9°C	25°C	9°C	25°C
	$RH_{initial}$	60%	60%	99.99%	99.99%	99.99%
	$w_{initial}$	17.6 kg/m³	17.6 kg/m³	160 kg/m³	160 kg/m³	160 kg/m³
Mineral wool	$T_{initial}$	25°C	15°C	25°C	15°C	25°C
	$RH_{initial}$	60%	60%	60%	60%	60%
Gypsum board	$T_{initial}$	25°C	20°C	25°C	20°C	25°C
	$RH_{initial}$	60%	60%	60%	60%	60%

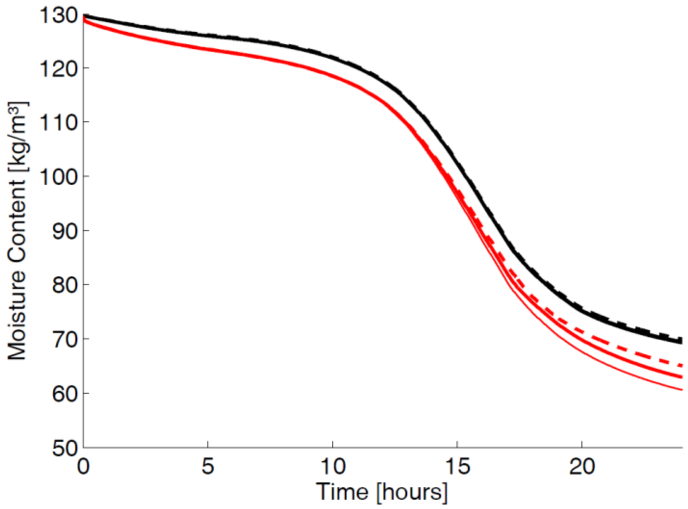

(a) Moisture content brick

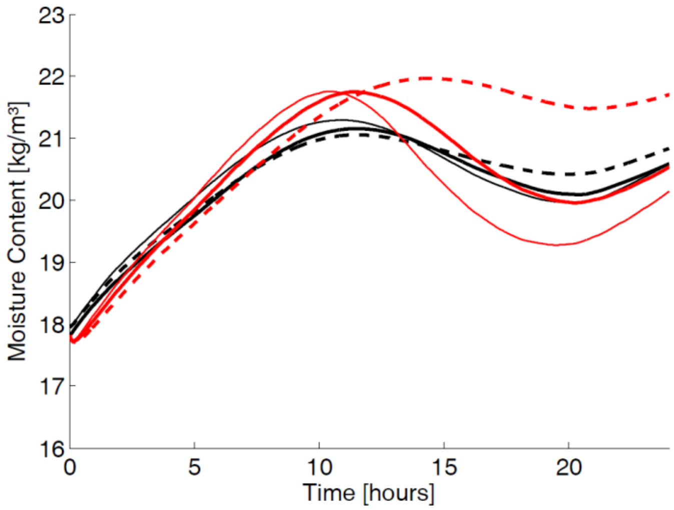

(b) Moisture content wood fibre board

Figure 8. Case 1: the moisture content in the brick and wood fibre board for a summer day, starting from saturated brick veneer and relatively dry wood fibre board. Comparison of the coupled CFD-HAM model (0.1m/s- -, 0.2m/s-, 0.3m/s-) and WUFI® (0.1m/s- -, 0.2m/s-, 0.3 m/s-)

Table 3. Relative difference of predicted moisture content between WUFI® and CFD-HAM model.

		Brick	Wood Fibre Board
Case 1	0.1m/s	7%	6%
	0.2m/s	9.4%	2.8%
	0.3m/s	12.4%	3.7%
Case 2		1.9%	8.4%
Case 3		9.1%	23.6%
Case 4		1.9%	14.5%

Figure 8 also shows the impact of the ventilation rate on the drying of the cavity wall. The coupled CFD-HAM model indicates that the effect of the ventilation rate is limited: varying the inlet velocity from 0.1 to 0.3 m/s showed almost no change in the drying course of the brick veneer. This seems reasonable since transfer rates to the outside are almost a magnitude higher. The drying potential of

the cavity for the ceramic brick can thus be considered small. The same conclusion was found by Hens et al. (2007).
The simplified model, however, shows a stronger impact of the ventilation in the cavity causing the brick veneer to dry faster if higher ventilation rates are present. Table 3 shows that at higher velocities, the deviation between both models becomes larger in the ceramic brick.
The wood fibre board at the inner leaf of the cavity behaves differently from the brick. Figure 8(b) compares the moisture content in the wood fibre board for the first simulation case. A variation in the moisture content is noticed: at first the moisture content increases, due to the high RH in the outside air. Next, the moisture content decreases as the cavity heats up. After 8 p.m., when solar radiation no longer reaches the wall, the temperature drops and the moisture content in the wood fibre board increases again. Both models show these trends. However, the variations predicted by the simplified model are larger than those predicted by the coupled CFD-HAM model.
Comparison of the relative difference of the moisture content in the wood fibre board (Table 3) shows no direct trend as function of the cavity velocity. However, Figure 8(b) does show increasing fluctuations in the moisture content of the wood fibre board for increasing cavity ventilation. The CFD-HAM model shows the same trends but less pronounced. It can thus also be stated for the wood fibre board that the simplified model overpredicts the effect of convection and that this overprediction increases as ventilation rates increase.
Table 3 indicates that the difference in predicted moisture content in the wood fibre board (between 2.8% and 6%) is smaller than in the brick (between 7% and 12.4%). This is because the brick starts from saturation, while the wood fibre board only contains hygroscopic moisture. When a saturated material is dried, drying will take place in the first drying stage. During the first drying stage, the drying rate is determined by the convection conditions. For the wood fibre board, however, moisture content is much lower and moisture is transported in the board by vapour diffusion. The moisture transfer from air to material and vice versa is in this case determined by the vapour diffusion properties of the porous material and less by the convection conditions in the air. In other words, the impact of convection is the largest for drying in the first drying stage. For hygroscopic loading, the impact of modelling the convection in a simplified way is less pronounced.

Case 2: winter conditions – non-saturated wood fibre board

Figure 9 shows the simulation results for the drying of a cavity wall under winter conditions. Because of the winter conditions applied in case 2, lower temperatures in the cavity wall are obtained which in turn results in lower drying rates compared to the first case.
Also, the RH in the air is higher for these winter conditions as can be seen in Figure 6. The drying course of the brick is mainly determined by the RH in the air. During a large part of the day, the RH is close to 100% and the brick leaf cannot dry out. The drying rate is no longer determined by the convection coefficients but by the humidity in the outside air. As a result, there is a better agreement between the simplified model and the CFD-HAM model (difference of only 1.9%).
For the wood fibre board, the difference between both models (8.4%) is larger than in the first case. Here, the wood fibre board is hygroscopically loaded. During the whole day, the mass fraction in the cavity air is higher than in the wood fibre board and the moisture content of the board monotonically rises.
In the first drying case, periods of hygroscopic loading were altered with periods of drying. This way, the too high moisture content during loading is compensated by the too high drying rate during drying and the overall difference between both models is less for this case.

Cases 3 and 4: summer and winter conditions – saturated wood fibre board

In cases 3 and 4, not only the ceramic brick was initially saturated with water but also the wood fibre board. The moisture content in the wood fibre board predicted with the simplified model and with the CFD-HAM model is compared in Figure 10. Table 3 shows the remarkably higher maximum difference between both simulations. The relative difference increased from 2.8% to 23.6% in summer and from 8.4% to 14.5% in winter. The simplified model clearly predicts a faster drying at the cavity side. In the brick, this difference was less pronounced since the drying of the brick took place at two sides. For the wood fibre board, only drying at the cavity side is possible.

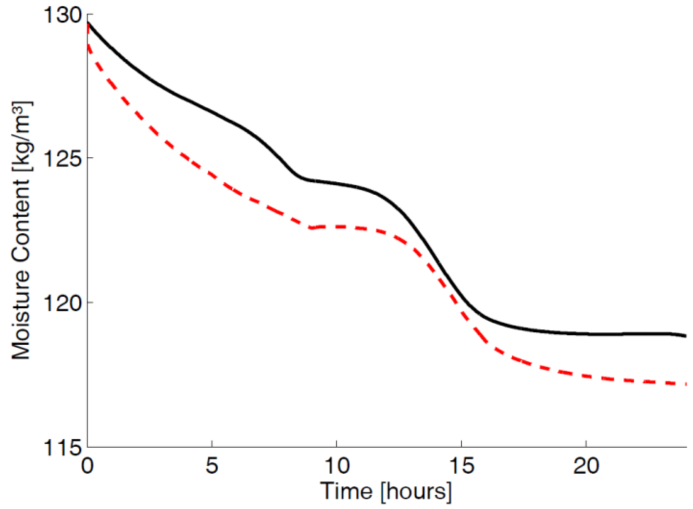

(a) Moisture content brick

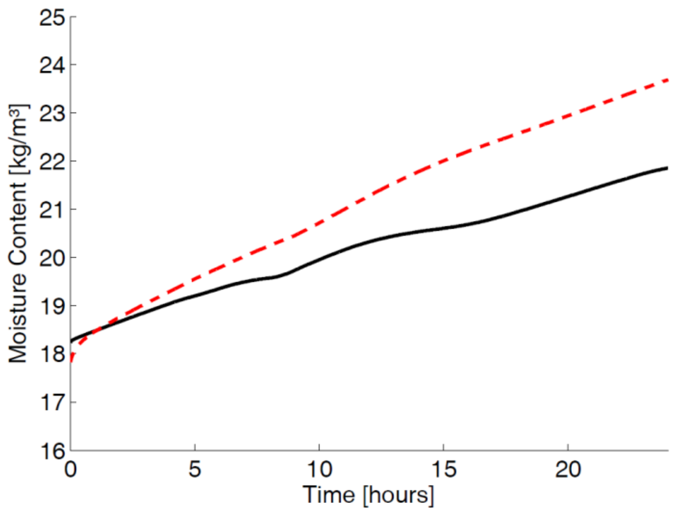

(b) Moisture content wood fibre board

Figure 9. Case 2: the moisture content in the brick and wood fibre board for a winter day starting from saturated brick veneer and relatively dry wood fibre board. Comparison of the coupled CFD-HAM model (-) and WUFI® (- -)

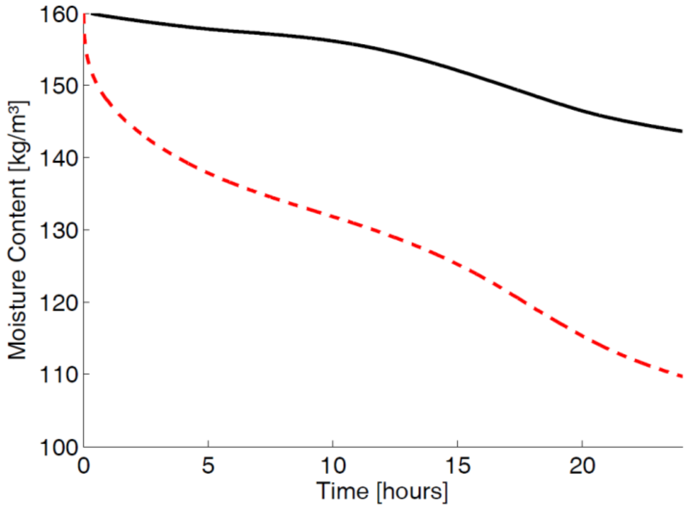

(a) Case 3: Moisture content of initially wet wood fibre board during a summer day

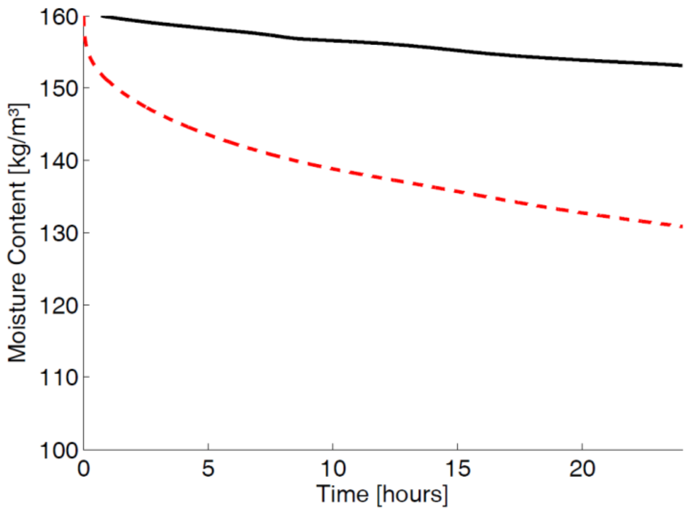

(b) Case 4: Moisture content of initially wet wood fibre board during a winter day

Figure 10. The drying course of a wet wood fibre board plate in a cavity wall under summer (case 3) and winter (case 4) conditions. Comparison between the coupled CFD-HAM model (-) and WUFI® (- -)

Case 5: comparison between constant velocity and constant pressure at the bottom of the cavity

In cases 1–4 that were discussed up till now, a constant inlet velocity was assumed based on the observations of Straube and Finch (2009). In reality, air movement in the cavity is induced by both the wind pressure ΔP_{wind} and the buoyancy-induced pressure ΔP_{stack}. The wind pressure depends on the environmental conditions such as outside wind speed, building orientation, location and building height. The stack pressure depends on temperature and moisture concentration distributions in the cavity. The pressure drop over the whole cavity will equal the driving force for pressure.

$$\Delta P_{tot} = \Delta P_{wind} + \Delta P_{stack} = C_{in}\frac{\rho v^2}{2} + f\phi v 4\frac{l}{D_h}\frac{\rho v^2}{2} + C_{out}\frac{\rho v^2}{2} \tag{25}$$

$$f = \frac{16}{Re} \tag{26}$$

In equation (25), f is the friction factor (–), given by equation (26) for laminar flow, ϕ is a correction factor for non-circular ducts (=1.5 for parallel plates; Verein Deutsche Ingenieure, 1994), D_h is the hydraulic diameter (m) (equal to twice the cavity width for parallel plates), v is the velocity in the cavity (m/s), ρ is the air density (kg/m^3) and C_{in} and C_{out} (–) are the pressure coefficients at the cavity inlet and outlet, respectively.

Thus, for a realistic case, the velocity and air flow rate in the cavity will not be constant over time. To study the effect of buoyancy on the flow rate in the cavity, a case is modelled for which a constant pressure at the bottom of the cavity is assumed (case 5 in Table 2). A pressure of 0.06 Pa is chosen, which corresponds with the pressure drop over the cavity when the inlet velocity would be 0.2 m/s and no buoyancy effects are present. The remaining boundary conditions are identical to the ones described in case 3.

It is thus possible to determine the ventilation rate in the cavity if the driving pressure difference ΔP_{tot} is known. This pressure difference is, however, strongly dependent on environmental conditions. Not only wind pressure fluctuates in time, since wind speed and direction change, but also the buoyancy-driven pressure difference changes as temperature and moisture concentrations change in the cavity over time. Straube and Finch (2009) showed the effect of changing environmental temperature and radiation on the ventilation rates in a cavity. They found that the ventilation rate in a cavity is to a great extent determined by buoyancy.

Figure 11 shows the average velocity at the bottom of the cavity over time. This clearly shows the variation in time of the velocity in the cavity. Variations can be so strong that the flow in the cavity changes direction. Positive velocities indicate a flow from bottom to top, and negative velocities indicate flow from top to bottom. The reversed flow is caused by the stack effect and can be explained by the outside climatic conditions. During the night, outside temperatures are low and no solar radiation is present. Still the wet brick wall and wood fibre board are slowly drying, causing the air temperature in the cavity to drop even further. The cold air is denser and forces a downward flow in the cavity. As the sun comes up, outside air temperature increases and radiation heats up the wall and cavity. Buoyancy forces move the air upwards in the cavity and around 9:00 a.m. the stack effect is strong enough to force the air upwards in the cavity. When evening falls, the temperature drops again, radiation disappears and the flow is again reversed.

Figure 12(a) compares the evolution in time of the moisture content in the brick wall for case 3 (constant inlet velocity) and case 5 (constant inlet pressure). Both simulated were performed with the coupled CFD-HAM model. The results show that the impact of the cavity ventilation on the drying of the brick wall is small. This indicates that a correct modelling of the convection in the cavity is not important when studying the drying behaviour of the outside leaf. This does not count for the inside leaf. Figure 12(b) clearly shows a deviation in drying behaviour for the wood fibre board when comparing both simulated cases. The wood fibre board initially dries faster for case 3 since in the first few hours air velocities in the cavity are higher in this case. However, after about 10 h, the velocity in the cavity is higher for case 5. This clearly results in a faster drying rate of the wood fibre board.

Simulation case 5 clearly illustrates the abilities of the newly developed coupled model. When ventilated cavity walls are studied in detail, a strong coupling exists between the heat and mass transport in the porous walls and the flow conditions in the cavity.

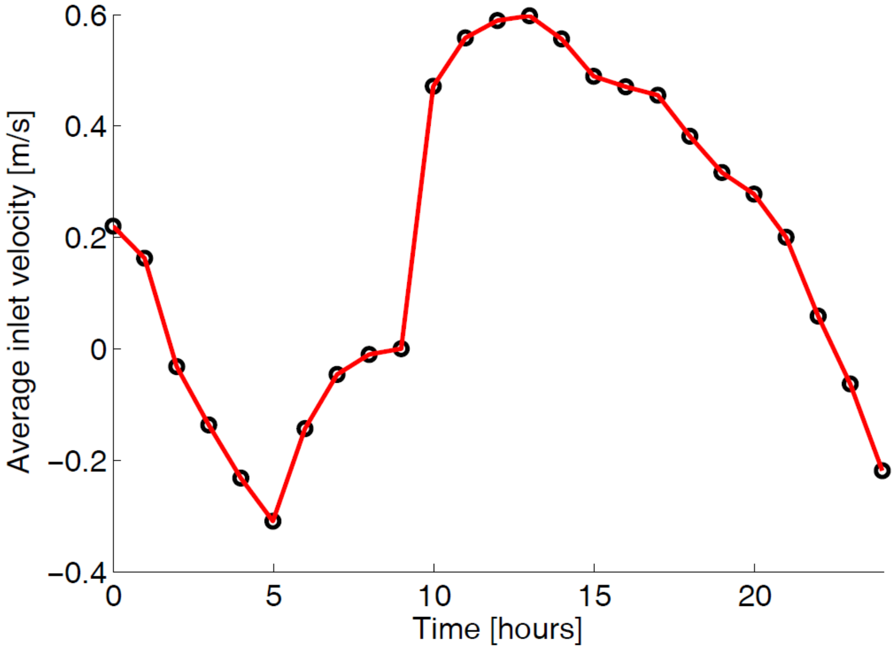

Figure 11. Average inlet velocity during 24 hours when a constant inlet pressure of 0.06 Pa is assumed at the bottom of the cavity. Positive velocities indicate a flow from bottom to top, negative velocities indicate a reverse flow.

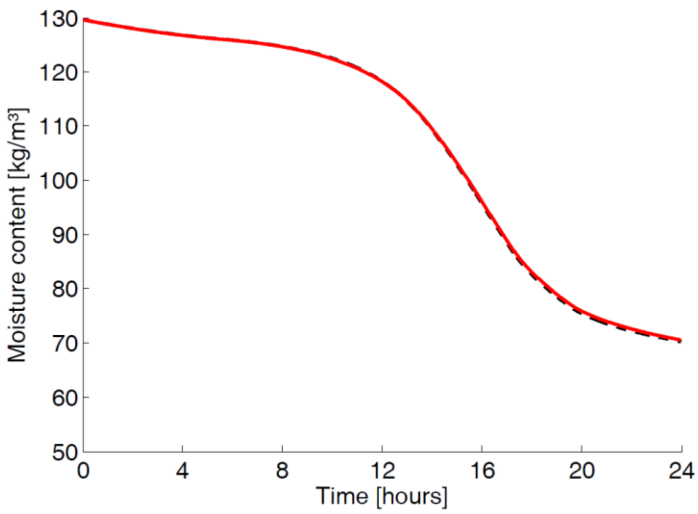

(a) Moisture content brick

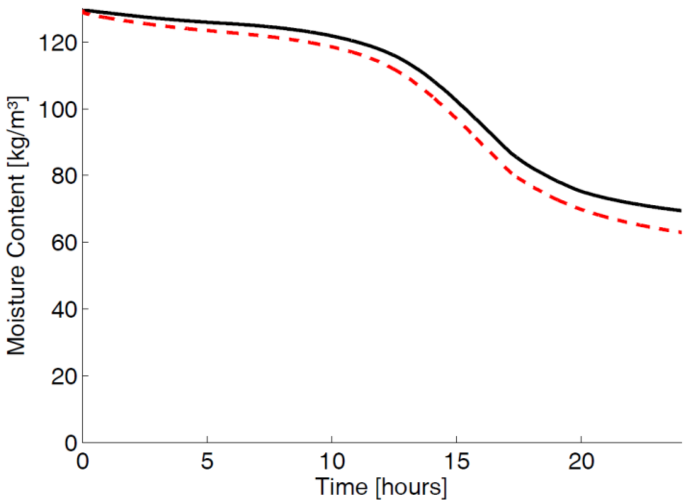

(b) Moisture content wood fibre board

Figure 12. Case 5: comparison of the moisture content in brick (a) and in wood fibre board (b) for summer conditions, with a constant velocity of 0.2 m/s (- -) and a constant pressure of 0.06 Pa at the bottom (--)

Conclusion

The analysis in this article showed some of the capacities of the newly developed coupled CFD-HAM model. The model allows a more detailed study of the complex heat and moisture transfer mechanisms in ventilated cavity walls. In existing commercial models, convection in the cavity was often modelled in a simplified way. This study showed that these simplifications are not always justified. To study the impact of the simplified convection modelling in a cavity, a comparison was made between WUFI that uses a simple convection model and the newly developed coupled CFD-HAM model that models convection uncompromised.

Both models showed that the drying of the outer leaf is mainly determined by the outside conditions and dries out mainly to the outside and not to the cavity. The cavity ventilation in this case is of less importance. For the wood fibre board leaf at the inside, the cavity ventilation is of major importance for drying. The study showed that the largest discrepancies between both models were found for this inner cavity leaf. The comparison also showed that the simplified model systematically overestimates the drying and moistening rates of the cavity wall. Differences in predicted moisture content up to 23.6% are registered. Winter conditions resulted in less severe differences, because for these cases the high RH of the outside air limits the drying rates. The largest discrepancies were found for simulations in summer conditions at the inside leaf when this leaf was initially saturated.

This shows that simplified models should be used carefully. Overestimating drying rates results in hazardous situations going unnoticed. Simulation results obtained with a simplified model may indicate in that case lower moisture contents than in reality, and consequently lower risk for mould growth, wood rot or other structural damage.

Furthermore, simplified models such as WUFI use a constant inlet air velocity as the boundary condition for the air cavity. In reality, air movement in the cavity is induced both by the wind pressure and by buoyancy effects, and thus, using a constant inlet air pressure would be more realistic. Detailed simulations with the CFD-HAM model showed that air velocities in the cavity may strongly vary and may even change direction. In this study, the impact of both types of boundary conditions on the drying rate of the cavity wall was also looked at. Simulations with the coupled CFD-HAM model have shown that a correct modelling of the convection in the cavity is of minor importance when looking at the drying behaviour of the outside leaf. However, for the inside leaf, the drying behaviour is influenced by the air velocity in the cavity.

The above study shows that when ventilated cavity walls are studied in detail, a strong coupling exists between the heat and mass transport in the porous walls and the flow conditions in the cavity. By consequence, the use of a simplified model is not always justified when evaluating the drying potential of a ventilated cavity, and in some cases, a correct evaluation of ventilated cavity walls is only possible if convection is modelled in detail. The newly developed coupled CFD-HAM model allows such evaluation.

Funding
The results presented in this article were obtained within the frame of the research project IWT-SB/81322/Van Belleghem funded by the Flemish Institute for the Promotion and Innovation by Science and Technology in Flanders. Their financial support is gratefully acknowledged.

References

- Defraeye T, Blocken B and Carmeliet J (2012) Analysis of convective heat and mass transfer coefficients for convective drying of a porous flat plate by conjugate modelling. International Journal of Heat and Mass Transfer 55(1–3): 112–124.
- Derluyn H, Janssen H, Moonen P, et al. (2008) Moisture transfer across the interface between brick and mortar joint. In: Proceedings of the 8th symposium on building physics in the Nordic Countries, Copenhagen, 16–18 June.
- Desta TZ, Langmans J and Roels S (2011) Experimental data set for validation of heat, air and moisture transport models of building envelopes. Building and Environment 46(5): 1038–1046.
- Finch G and Straube J (2007) Ventilated wall claddings: review, field performance and hygrothermal modeling. In: Proceedings of the thermal performance of the exterior envelopes of whole buildings X, Clearwater, FL, 2 December 2007.
- Fluent Inc. (2006) Fluent 6.3 User’s Guide. Lebanon, NH: Fluent Inc.
- Ge H and Ye Y (2007) Investigation of ventilation drying of rainscreen walls in the coastal climate of British Columbia. In: Proceedings of the thermal performance of the exterior envelopes of whole buildings X, Clearwater, FL, 2 December 2007.
- Hens H (1997) Bouwfysica 1: Warmte en Massatransport (in Dutch). Leuven: ACCO.
- Hens H (2007) Building Physics – Heat, Air and Moisture: Fundamentals and Engineering Methods with Examples and Exercises. Berlin: Ernst & Sohn.
- Hens H, Janssens A, Depraetere W, et al. (2007) Brick cavity walls: a performance analysis based on measurements and simulations. Journal of Building Physics 31(2): 95–124.
- ISOPROC. http://www.isoproc.be, website consulted on August 10, 2012.
- Janssen H (2011) Thermal diffusion of water vapour in porous materials: fact or fiction? International Journal of Heat and Mass Transfer 54(7–8): 1548–1562.
- Janssen H, Blocken B and Carmeliet J (2007) Conservative modelling of the moisture and heat transfer in building components under atmospheric excitation. International Journal of Heat and Mass Transfer 50(5–6): 1128–1140.
- Jung E (1985) Long-term performance of facing masonry exposed to the weather and the effect of cavity insulation. Results of tests carried out in laboratory and on buildings. Baustoffindustrie 28(6): 185.
- Karagiozis AN and Ku¨ nzel HM (2009) The effect of air cavity convection on the wetting and drying behavior of wood-frame walls using a multi-physics approach. Journal of ASTM International 6(10): 1–15. DOI: 10.1520/JAI101455.
- Künzel HM, Hens H, Karagiozis A, et al. (2009) Chapter 25. Heat, air and moisture control in building assemblies – fundamentals. In: ASHRAE (ed.) ASHRAE Handbook – Fundamentals. Atlanta, GA: ASHRAE.
- Meteotest (2012) Meteonorm: global meteorological database. Available at: http://www.meteonorm.com

- Roels S (2008) IEA Annex41 whole building heat, air and moisture response – subtask 2: experimental analysis of moisture buffering. Technical report, 19 June. France: International Energy Agency (IEA).
- Salonvaara M, Karagiozis AN, Pazera M, et al. (2007) Air cavities behind claddings – what have we learned? In: Proceedings of the thermal performance of the exterior envelopes of whole buildings X, Clearwater, FL, 2 December 2007.
- Saneinejad S, Moonen P, Defraeye T, et al. (2012) Coupled CFD, radiation and porous media transport model for evaluating evaporative cooling in an urban environment. Journal of Wind Engineering and Industrial Aerodynamics 104–106: 455–463.
- Sanjuan C, Jose Suarez M, Blanco E, et al. (2011) Development and experimental validation of a simulation model for open joint ventilated facades. Energy and Buildings 43(12): 3446–3456.
- Schirmer R (1938) Die Diffusionszahl von Wasserdampf-Luftgemischen und die Verdampfungsgeschwindigkeit. VDI Beiheft Verfahrestechnik 6: 170–172.
- Steeman HJ (2008) Modelling local hygrothermal interaction between airflow and porous materials for building applications. PhD Thesis, Ghent University, Ghent.
- Steeman HJ, Van Belleghem M, Janssens A, et al. (2009) Coupled simulation of heat and moisture transport in air and porous materials for the assessment of moisture related damage. Building and Environment 44(10): 2176–2184.
- Straube J (1998) Moisture control and enclosure wall systems. PhD Thesis, University of Waterloo, Waterloo, ON, Canada.
- Straube J and Finch G (2009) Ventilation wall claddings: review, field performance and hygrothermal modeling. Technical report-0906. Westford, MA: Building Science Corporation.
- Van Belleghem M, Steeman H-J, Steeman M, et al. (2010) Sensitivity analysis of CFD coupled non-isothermal heat and moisture modelling. Building and Environment 45(11): 2485–2496.
- Van Belleghem M, Steeman M, Janssen H, et al. (2014) Validation of a coupled heat, vapour and liquid transport model for porous materials implemented in CFD. Building and Environment.
- Van Belleghem M, Steeman M, Willockx A, et al. (2011) Benchmark experiments for moisture transfer modelling in air and porous materials. Building and Environment 46(4): 884–898.
- Verein Deutsche Ingenieure (1994) VDI Wärmeatlas: Berechnungsblätter für den Wärmeübergang. 7th ed. Dusseldorf: VDI Verlag.
- Versteeg HK and Malalasekara W (2007) An Introduction to Computational Fluid Dynamics: The Finite Volume Method. Essex: Pearson Education Limited.
- Waananen KM, Litchfield JB and Okos MR (1993) Classification of drying models for porous solids. Drying Technology 11(1): 1–40.
- Welty JR, Wicks CE, Wilson RE, et al. (2001) Fundamentals of Momentum, Heat and Mass Transport. New York: John Wiley & Sons, Inc.
- Whitaker S (1988) The role of irreversible thermodynamics and the Onsager relations in the analysis of drying phenomena. In: Proceedings of the sixth international drying symposium IDS'88, Versailles, September.
- Zirkelbach D, Schmidt T, Kunzel HM, et al. (2007) WUFI 2D Installation and Introduction, Fraunhofer Institute for Building Physics.

Appendix 1

Moisture transport properties of ceramic brick

The material properties of ceramic brick were experimentally determined by Derluyn et al. (2008).

Vapour diffusion coefficient

$$\delta_v = \frac{2.61\times10^{-5}}{\kappa_{dry} R_v T} \frac{1-(w/w_{cap})}{0.503\left(1-(w/w_{cap})\right)^2+0.497} \quad (27)$$

Table 4. Coefficients in equation (27)

	a	n	m	w
1	1.35×10^{-5}	6	0.8333	0.36
2	4×10^{-6}	2	2	0.25
3	5×10^{-7}	0.7	0.4	0.39

Moisture retention curve

$$w(p_c) = w_{cap}\left[\begin{matrix}0.846(1+(1.394\times10^{-5}p_c)^4)^{-0.75} + \\ 0.154(1+(0.9011\times10^{-5}p_c)^{1.69})^{-0.408}\end{matrix}\right] \quad (28)$$

Liquid permeability

$$K_l = K_s[\sum_{i=1}^{3} w_i(1+(-a_i p_c)^{n_i})^{-m_i}]^{\tau}\left[\frac{\sum_{i=1}^{3} a_i w_i\left(1-\left[\frac{(-a_i p_c)^{n_i}}{1+(-a_i p_c)^{n_i}}\right]^{m_i}\right)}{\sum_{i=1}^{3} a_i w_i}\right]^2 \quad (29)$$

With $K_s=1.15\times10^{-9}$ and $\tau=4.003$. The values for a_i, n_i, m_i and w_i are listed in Table 4.

Moisture transport properties of wood fibre board (Celit)

The material properties of wood fibre board are found in Desta et al. (2011).

Retention curve

$$w = \left[1+\left(\frac{m p_c}{R_v T \rho_{liq}}\right)^n\right]^{\frac{1-n}{n}} \quad (30)$$

With

$m = -900$

$n = 1.36$ (31)

Liquid permeability

$$K_l = D_w \frac{\partial w}{\partial p_c} \quad (32)$$

$$D_w = 3.8\left(\frac{a}{w_{sat}}\right)^2 1000^{\left(\frac{w}{w_{sat}}-1\right)} \quad (33)$$

With

$a = 0.0052$

$w_{sat} = 162\ kg/m^3$ (34)

Moisture transport properties of gypsum board

The material properties of gypsum board were taken from ANNEX 41 (Roels, 2008).

Water vapour resistance factor

$$\mu = \frac{\mu_0}{1+aRH^n} \quad (35)$$

With

$\mu_0 = 10.68205$
$a = 1.229557$
$n = 2.983921$
(36)

Sorption isotherm
The following equation was used by Steeman (2008) based on the measurement data in Roels (2008)

$$w_a = \frac{RH}{aRH^2 + bRH + c} \tag{37}$$

With
$a = -0.81655$
$b = 0.85157$
$c = 0.011176$ (38)

Appendix 2
Notation

Symbol	Description	Unit
C	Specific heat capacity	J/kgK
C_{in}, C_{out}	Pressure coefficient	-
D_h	Hydraulic diameter	m
dr_a	Distance from the air-material interface to the cell centre	m
D_{va}	Diffusivity of water vapour in air	m^2/s
E	Total energy	J
f	Friction factor	-
g	Moisture flux	kg/m^2s
h	Specific enthalpy	J/kg
K_l	Liquid permeability	s
L	Latent heat	J/kg
P	Pressure	Pa
p_c	Capillary pressure	Pa
p_v	Partial vapour pressure	Pa
Pr	Prandtl number	-
Q_{air}	Air change rate	1/s
q	Heat Flux	W/m^2

Re	Reynolds number	-
RH	Relative humidity	-
R_v	Specific gas constant of water vapour	J/kgK
S	Source/Sink	-
Sc	Schmidt number	-
T	Temperature	K
v	velocity	m/s
w	Moisture content	kg/m^3
Y	Mass fraction	kg/kg
Greek symbols		
α	Heat transfer coefficient	W/m^2K
β	Mass transfer coefficient	s/m
δ	Diffusion coefficient	s
ε	Emissivity	-
λ	Heat conductivity	W/mK
μ	Water vapour resistance factor	-
ν	Kinematic viscosity	m^2/s
ρ	Density	kg/m^3
ψ_0	Open porosity	-
f	Correction factor	-
Subscripts		
a	Air	
avg	Average	
cap	Capillary	
eff	Effective	
in	Inlet	

l	Liquid
mat	Material
op	Operating
out	Outlet
rad	Radiation
ref	Reference
s	Surface
sa	Surface facing the air side
sm	Surface facing the material side
sat	Saturation
t	Turbulent
tot	Total
v	Vapour